# CHAPTER IV
# RESULTS AND DISCUSSION

## 4.1 Characterization of Adsorbent

### 4.1.1 Water Content Analysis

Many literatures suggest that water content in an adsorbent has the effect on the competitive adsorption. The more the water content, the less the adsorption capacity of metallic mercury. In order to minimize the effect of water content, adsorbents must be preheated before use. The preheating temperature was determined by thermogravimetric analysis (TGA).

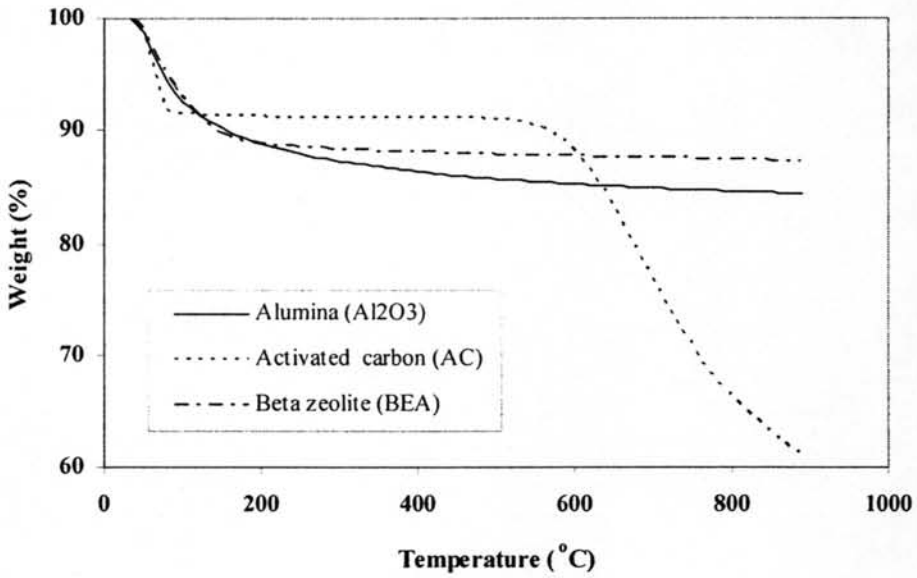


**Figure 4.1** Thermograms of alumina, activated carbon, and Beta zeolite.

TGA results (Figure 4.1) shows weight in percent with increased temperature of the supports for alumina, activated carbon, and Beta zeolite. The weight was rapidly decreased when temperature reached around 70°C and became constant at around 350°C for both alumina and Beta zeolite. For activated carbon, the weight became constant at around 200°C. The rapidly decreased curve at temperature around 100°C was due to water desorption. Therefore, alumina and Beta zeolite were

preheated at 350°C while activated carbon was preheated at 200°C for 10 h (Table 4.1 shows water content in alumina, activated carbon, and Beta zeolite). In case of CuS impregnated adsorbents, it was used directly without preheating because preheating can cause the loss of adsorbent material (Ullah, 2006). Therefore, CuS impregnated adsorbents were kept in a desiccator to prevent water adsorption from the atmosphere.

**Table 4.1** Water content in the supports

| Support | Water content (wt %) |
|---|---|
| Alumina | 13.24 |
| Activated carbon | 8.78 |
| Beta zeolite | 11.83 |

4.1.2 Atomic Absorption Spectroscopy (AAS)

The CuS adsorbents were also analyzed for copper content on the support by using Atomic Absorption Spectrometer (AAS). The results of copper content are shown in Table 4.2.

**Table 4.2** Copper content on the CuS adsorbents

| Adsorbent | Cu content (wt %) |
|---|---|
| CuS/BEA | 13.32 |
| $CuS/Al_2O_3$ | 11.97 |

4.1.3 X-Ray Diffraction (XRD) Spectrometer

The results of the powder XRD patterns of the CuS adsorbents are shown in Figure 4.2. The positions and intensities of the diffraction peaks are in good agreement with the literature value for CuS covellite, syn (JCPDS files No. 06-0464).

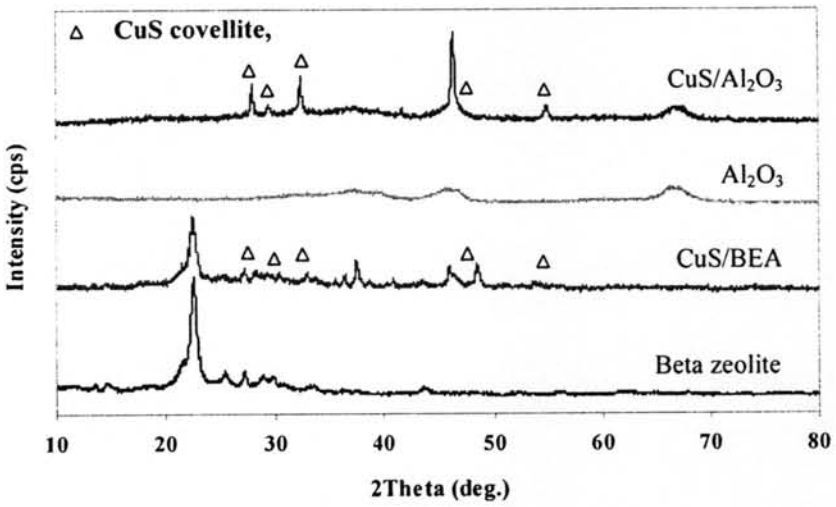


**Figure 4.2** XRD patterns of the CuS adsorbents.

### 4.2 Blank Test

The experiment in this section was conducted to study the stability of metallic mercury at temperature of 50°C. The time in this section covered the time in adsorption kinetic part and adsorption isotherm part. The result (Figure 4.3) shows only 2.60% loss of metallic mercury in a 20 ml glass vial for 8 h. This indicates that the metallic mercury does not adsorb on the glassware or disappear by vaporization. The difference of concentration found is considered as the error in measurement analysis. Therefore, the adsorption capacities of metallic mercury in the adsorption kinetic part and the adsorption isotherm part are caused by the adsorption property of the adsorbents.

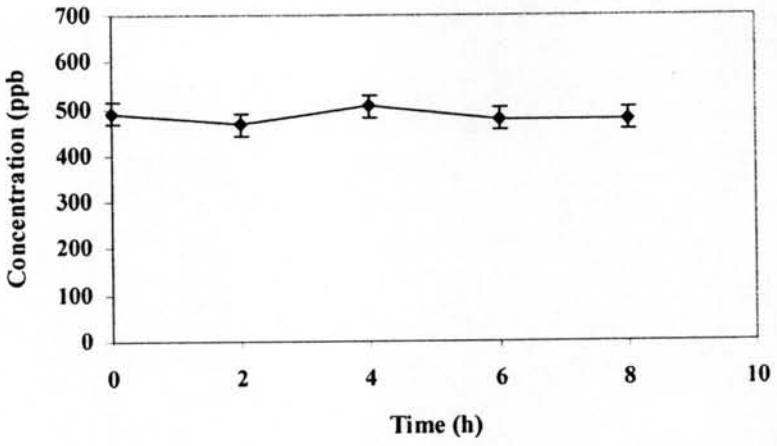


**Figure 4.3** Remaining concentration of metallic mercury solution of 500 ppb in the study on blank test at temperature 50°C.

### 4.3 Appropriate Quantity of Adsorbent

The adsorption capacities of the different quantities of adsorbent varied between 0.001 g and 0.1 g (0.001, 0.01, 0.05, and 0.1 g) were shown in Figure 4.4. The adsorption capacity increased rapidly between 0.001 g and 0.01 g of adsorbent and then reached the maximum when the amount of adsorbent was more than 0.01 g. In addition, the difference between the adsorption capacity on $CuS/Al_2O_3$ and CuS/BEA was observed at 0.001 g of adsorbent. To study the capability of the adsorbent in the metallic mercury adsorption, 0.001 g of adsorbent was used in the experiments.

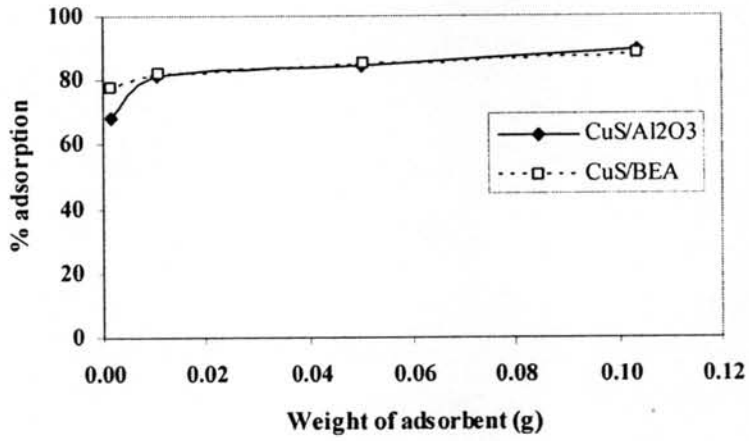


**Figure 4.4** Effect of adsorbent quantity on the adsorption capacity of metallic mercury at 500 ppb, 50°C, and equilibrium time 6 h.

### 4.4 Adsorption Kinetic Study

The adsorption kinetics of metallic mercury on supports – Beta zeolite, alumina, and activated carbon – and copper sulfide (CuS) on these supports such as $CuS/Al_2O_3$ and CuS/BEA were studied. The experiments were conducted with 500 ppb of metallic mercury in heavy naphtha at 50°C. The results (Figure 4.5) show that equilibrium is attained at about 50 min for alumina and Beta zeolite and 200 min for activated carbon. The adsorption capacity was in the decreasing order of; activated carbon (24%) > Beta zeolite (13%) > alumina (9%) removal were achieved. This may be due to higher surface area of activated carbon (1150-1250 $m^2/g$) than Beta zeolite (636 $m^2/g$) and alumina (274 $m^2/g$). Moreover, the non-polar molecules of metallic mercury preferred to adsorb on the surface of activated carbon which is non-polar. The result conformed with that of Dunham *et al.* (2003) who suggested that surface area as well as nature of the surface are important for adsorption of metallic mercury.

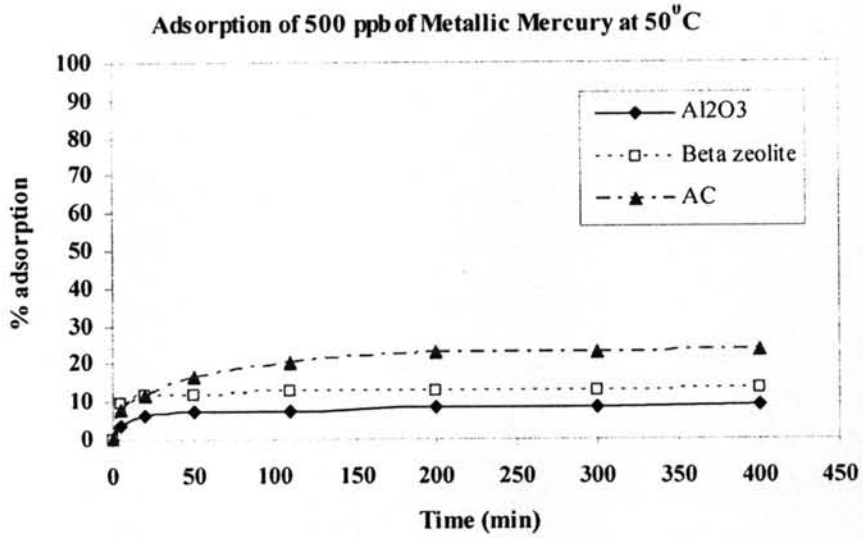


**Figure 4.5** Kinetics of adsorption of metallic mercury on the supports for concentration 500 ppb at 50°C.

In order to improve the mercury removal efficiency, the impregnation of copper sulfide (CuS) on supports was studied. The results (Figure 4.6) show better mercury removal by CuS adsorbents than virgin ones, as shown on $CuS/Al_2O_3$ and CuS/BEA that 96% and 98% adsorption were achieved, respectively. This may be due to mercury reactive materials (CuS) to form the reaction with metallic mercury molecules. For CuS adsorbents, chemisorption was facilitated by the formation of mercuric sulfide (HgS) while physisorption was a dominant process using virgin adsorbents. Furthermore, the shape of adsorption of CuS adsorbents was quite similar as that of CMG273 which 94% adsorption was achieved at about 300 min. The result for CMG273 showed a lower adsorption capacity than that of a previous work (Fahim, 2006) which 97% adsorption was achieved using CMG273 for removing metallic mercury from n-heptane. This was due to the complexity of various hydrocarbons in heavy naphtha that affected the competitive adsorption on CMG273.

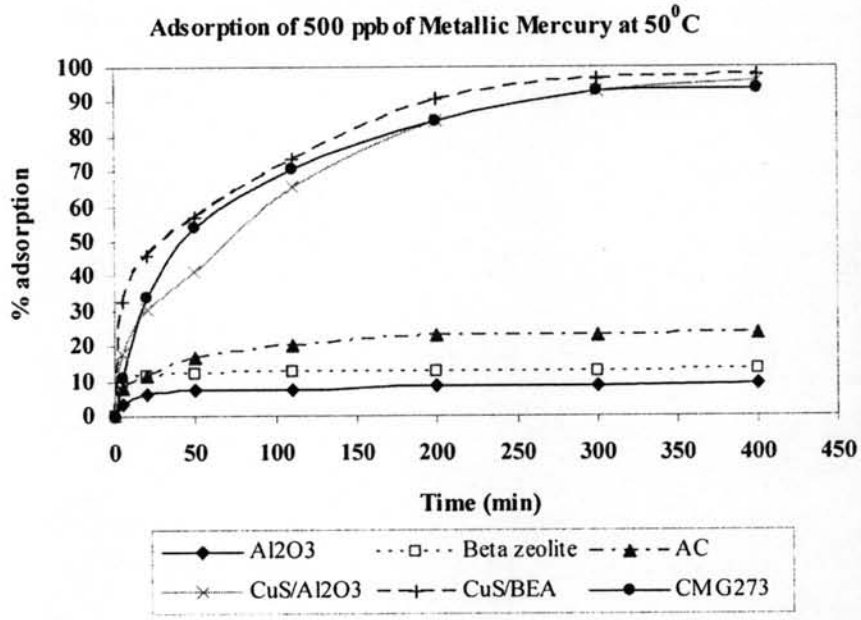


**Figure 4.6** Kinetics of adsorption of metallic mercury at concentration 500 ppb and 50°C.

## 4.5 Kinetic Models

There are three kinetic models that have been used to explain the kinetic data: the pseudo first order equation, the pseudo second order equation, and the intraparticle diffusion equation. All kinetic parameters were shown in Table 4.3.

### 4.5.1 The Pseudo First Order Equation

According to Eq. (2.15), the rate constants, $k_{p1}$, and correlation coefficients, $R^2$, were determined from the plot of log ($q_e$-$q_t$) against $t$ (Figure 4.7). However, this equation is valid only for the initial adsorption period. From the results, approximately linear fits were observed for all adsorbents, indicating that the adsorption can be approximated to pseudo first order kinetics. Constants $k_{p1}$ for all adsorbents were calculated and summarized in Table 4.3. These values indicate that the initial rate of metallic mercury removal of CMG273 is fastest among the all adsorbents.

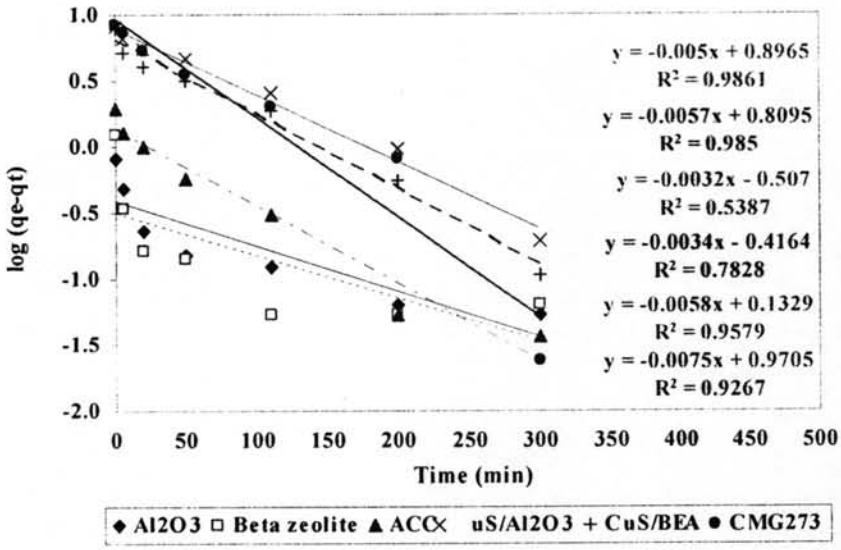


**Figure 4.7** Pseudo first order plot for metallic mercury removal at concentration 500 ppb and 50°C.

**Table 4.3** Kinetic parameters for the removal of metallic mercury

**Pseudo first order constants**

| Adsorbent | $q_{e,exp}$ (mg/g) | $q_{e,cal}$ (mg/g) | $k_{p1}$ ($min^{-1}$) | $R^2$ |
|---|---|---|---|---|
| $Al_2O_3$ | 0.8137 | 0.3834 | 0.0078 | 0.7828 |
| $CuS/Al_2O_3$ | 8.1098 | 7.8795 | 0.0115 | 0.9861 |
| AC | 1.9492 | 1.3580 | 0.0134 | 0.9579 |
| Beta zeolite | 1.2339 | 0.3112 | 0.0074 | 0.5387 |
| CuS/BEA | 7.7298 | 6.4491 | 0.0131 | 0.9850 |
| CMG273 | 8.3283 | 9.3433 | 0.0173 | 0.9267 |

**Pseudo second order constants**

| Adsorbent | $q_{e,cal}$ (mg/g) | $k_{p2}$ (g/mg min) | h (mg/g min) | $R^2$ |
|---|---|---|---|---|
| $Al_2O_3$ | 0.8164 | 0.0968 | 0.0645 | 0.9974 |
| $CuS/Al_2O_3$ | 9.1659 | 0.0020 | 0.1669 | 0.9862 |
| AC | 2.0446 | 0.0243 | 0.1016 | 0.9986 |
| Beta zeolite | 1.2238 | 0.1768 | 0.2648 | 0.9988 |
| CuS/BEA | 8.2440 | 0.0042 | 0.2828 | 0.9943 |
| CMG273 | 9.3371 | 0.0024 | 0.2053 | 0.9989 |

**Intraparticle diffusion constants**

| Adsorbent | $k_{id}$ (mg/g $min^{1/2}$) | $R^2$ |
|---|---|---|
| $Al_2O_3$ | 0.0323 | 0.7191 |
| $CuS/Al_2O_3$ | 0.4190 | 0.9725 |
| AC | 0.0906 | 0.8611 |
| Beta zeolite | 0.0394 | 0.4873 |
| CuS/BEA | 0.3615 | 0.9157 |
| CMG273 | 0.4371 | 0.9352 |

### 4.5.2 The Pseudo Second Order Equaiton

Figure 4.8 shows the plot of $t/q_t$ versus $t$ according to Eq. (2.17). The value of $q_e$ was obtained from the slope of the plot while $k_{p2}$ and $h$ were obtained from the intercept.

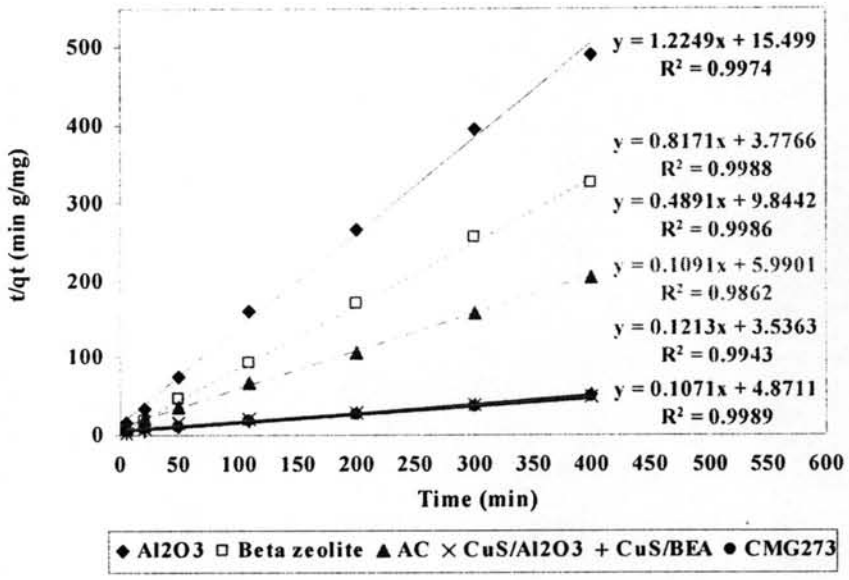


**Figure 4.8** Pseudo second order plot for metallic mercury removal at concentration 500 ppb and 50°C.

The $q_{e,exp}$ and the $q_{e,cal}$ values along with calculated correlation coefficients for pseudo first order model and pseudo second order model by using regression procedure for metallic mercury are shown in Table 4.3. The $q_{e,exp}$ and the $q_{e,cal}$ values from pseudo second order kinetics model were very close to each other. The calculated correlation coefficients were also closer to unity for pseudo second order

kinetics than for the pseudo first order kinetic model. Therefore, the adsorption reaction could be approximated more favorably by the pseudo second order kinetic model for all adsorbents. Values of $q_e$, $k_{p2}$ and $h$ as calculated from the Figure 4.8 are list in Table 4.3. It can be seen that the value of $q_e$ for CMG273 is highest. Thus, CMG273 had the highest affinity for metallic mercury removal but the initial rate ($h$) was highest for CuS on Beta zeolite (CuS/BEA).

### 4.5.3 The Intraparticle Diffusion Equation

According to Eq. (2.19), a plot of $q_t$ versus $t^{1/2}$ should be a straight line with a slope $k_{id}$ when adsorption mechanism follows the intraparticle diffusion process. Figure 4.9 shows the plot of $q_t$ versus $t^{1/2}$ for all adsorbents. The deviation of the straight lines from the origin (Figure 4.9) may be due to the difference in the rate of mass transfer in the initial and final stages of adsorption. Further, such deviation of the straight lines from the origin indicates that the pore diffusion is not rate controlling step. The values of $k_{id}$ as obtained from the slope of straight lines are listed in Table 4.3. CMG273 has the highest value of $k_{id}$ followed by $CuS/Al_2O_3$, CuS/BEA, activated carbon, Beta zeolite, and alumina in that order.

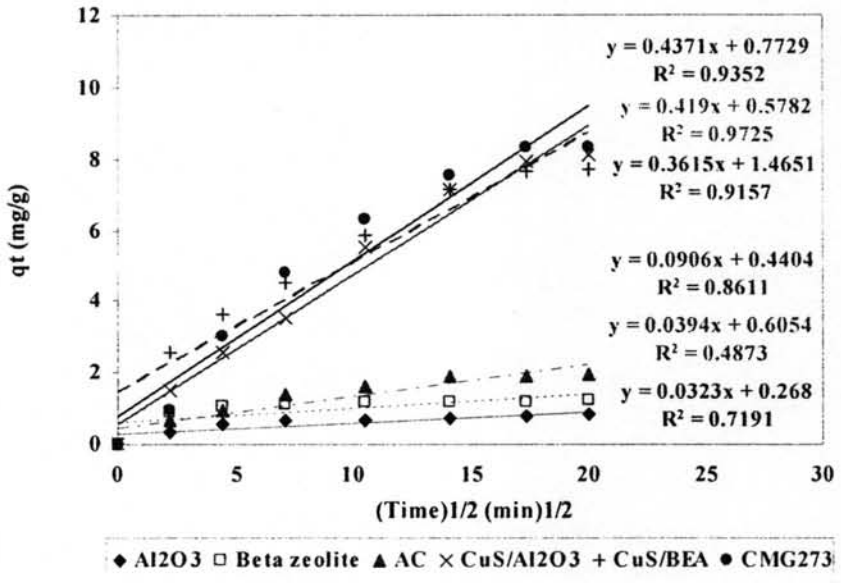


**Figure 4.9** Intraparticle diffusion plot for metallic mercury removal at concentration 500 ppb and 50°C.

Normally, solid-liquid adsorption processes are characterized by three consecutive steps, namely external diffusion, internal diffusion and the adsorption stage. The adsorption stage is usually fast and can be negligible. External diffusion involves the movement of adsorbate molecules from the bulk of the solution toward the surface of the adsorbent. This is followed by movement of molecules through the boundary layer while internal diffusion involves the movement of molecules in the interior of the particles. In the solid-liquid adsorption processes, there is always the involvement of the two mechanisms. For example, the first stage of the process is usually dominated by external diffusion which facilitates loading of the solute to the adsorbent before internal diffusion takes place. Therefore, it is essential to distinguish between external and internal diffusion. If the external transport is greater than the internal transport, then the rate is controlled by film diffusion and if the external transport is less than the internal transport, particle diffusion becomes the dominant mechanism.

Mohan and Singh (2002) maintained that external transport is the rate-limiting step in systems in which there is poor mixing, low concentration of adsorbate, small particle size and high affinity of adsorbate for the adsorbent. On the contrary, internal diffusion dominates in systems with high concentration of adsorbate, good mixing, large particle size of adsorbent and low affinity of adsorbate for the adsorbent.

In order to identify the slowest steps in the adsorption process, the Boyd kinetic equation (Mohan and Singh, 2002) was applied and it is represented as

$$F = 1 - \frac{6}{\pi^2}\exp\left(-\frac{\pi^2 D_i}{r_0^{\,2}}t\right) = 1 - \frac{6}{\pi^2}\exp(-Bt) \tag{4.1}$$

where $F = q_t/q_e$ is the fractional approach to equilibrium at time $t$ and $B$ is given as

$$B = \frac{\pi^2 D_i}{r_0^{\,2}} \tag{4.2}$$

$D_i$ is the effective diffusion coefficient of the solute in the adsorbent phase and $r_0$ is the radius of the adsorbent particles.

Eq. (4.2) can be rearranged while taking natural logarithm to obtain the equation

$$Bt = -0.4977 - \ln(1 - F) \tag{4.3}$$

The values of *Bt* can be evaluated for different time intervals using Eq. (4.3). A plot of *Bt* against *t* can be employed to test the linearity of the experimental values. If the plots are linear and passing through the origin, then the slowest step in the adsorption process is the internal diffusion and vice versa. The *Bt* against *t* plots are shown in Figure 4.10.

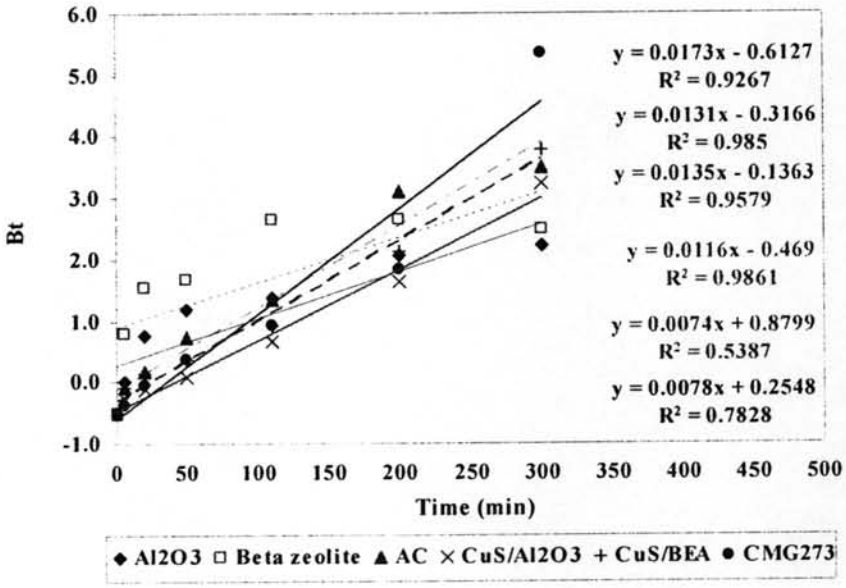


**Figure 4.10** Plot of *Bt* versus time for metallic mercury removal at concentration 500 ppb and 50°C.

It is apparent from the graphs that the *Bt* against *t* plots do not pass through the origin, hence the adsorption process is mainly controlled by film diffusion. The calculated effective diffusion coefficient ($D_i$) values on different adsorbents (Table 4.4) show that CuS/BEA has higher pore diffusion rate than $CuS/Al_2O_3$.

**Table 4.4** Effective diffusion coefficient for metallic mercury removal

| Adsorbent | Effective diffusion coefficient, $D_i$ ($m^2/s$) |
|---|---|
| $Al_2O_3$ | 2.06E-13 |
| $CuS/Al_2O_3$ | 3.06E-13 |
| AC | 3.56E-13 |
| Beta zeolite | 1.95E-13 |
| CuS/BEA | 3.46E-13 |
| CMG273 | 4.56E-13 |

## 4.6 Adsorption Isotherm Study

Isotherm studies were conducted at 50°C and an equilibrium time of 6 h by using $CuS/Al_2O_3$, CuS/BEA, and CMG273. Figure 4.11 shows adsorption isotherms of metallic mercury on $CuS/Al_2O_3$, CuS/BEA, and CMG273 at 50°C. Correlation of the data using empirical or theoretical equations is required in the analysis and design of an adsorption process. The BET, Freundlich, and Langmuir adsorption isotherm models, respectively, were examined in this study to describe the adsorption equilibrium.

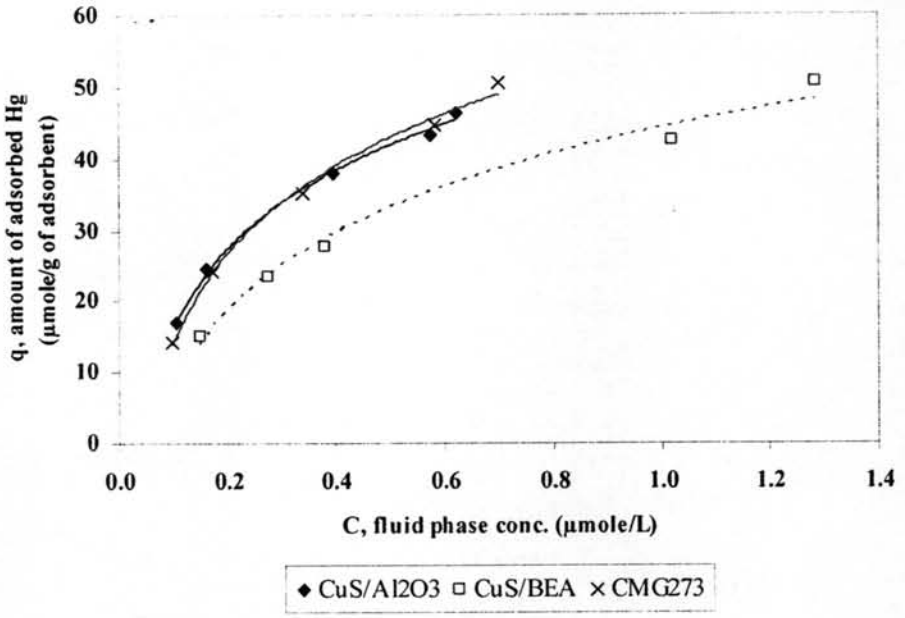


**Figure 4.11** Adsorption isotherms of metallic mercury at 50°C.

The BET, Freundlich, and Langmuir adsorption constants evaluated from the isotherms for different adsorbents and their correlation coefficients ($R$) are presented in Table 4.5 according to linear forms of Eq. (2.21), (2.23), and (2.25), respectively. The plots of linear forms are shown in Figure 4.12, 4.13, and 4.14 for BET isotherm, Freundlich isotherm, and Langmuir isotherm, respectively.

**Table 4.5** Isotherm constants and value of $R^2$ for metallic mercury removal

| **BET constants** | | | |
|---|---|---|---|
| Adsorbent | $K_B$ | $q_{max}$ (μmole/g) | $R^2$ |
| $CuS/Al_2O_3$ | 26.29 | 54.35 | 0.9955 |
| CuS/BEA | 18.00 | 46.30 | 0.9951 |
| CMG273 | 18.11 | 61.35 | 0.9926 |

| **Freundlich constants** | | | |
|---|---|---|---|
| Adsorbent | $K_F$ (μmole/g) | 1/n | $R^2$ |
| $CuS/Al_2O_3$ | 60.38 | 0.54 | 0.9835 |
| CuS/BEA | 44.03 | 0.53 | 0.988 |
| CMG273 | 64.55 | 0.61 | 0.9801 |

| **Langmuir constants** | | | |
|---|---|---|---|
| Adsorbent | b (L/μmole) | $q_{max}$ (μmole/g) | $R^2$ |
| $CuS/Al_2O_3$ | 3.13 | 69.44 | 0.9943 |
| CuS/BEA | 2.00 | 65.79 | 0.9974 |
| CMG273 | 2.11 | 84.75 | 0.9939 |

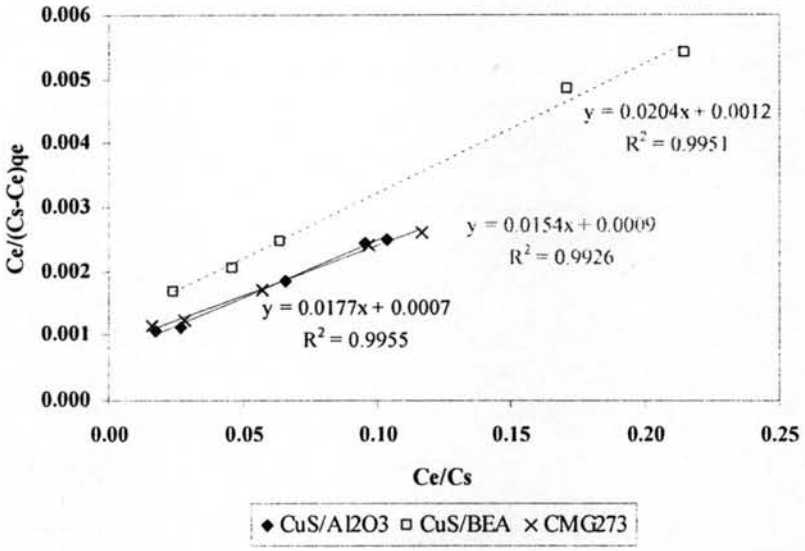


**Figure 4.12** BET adsorption isotherm for metallic mercury removal at 50°C.

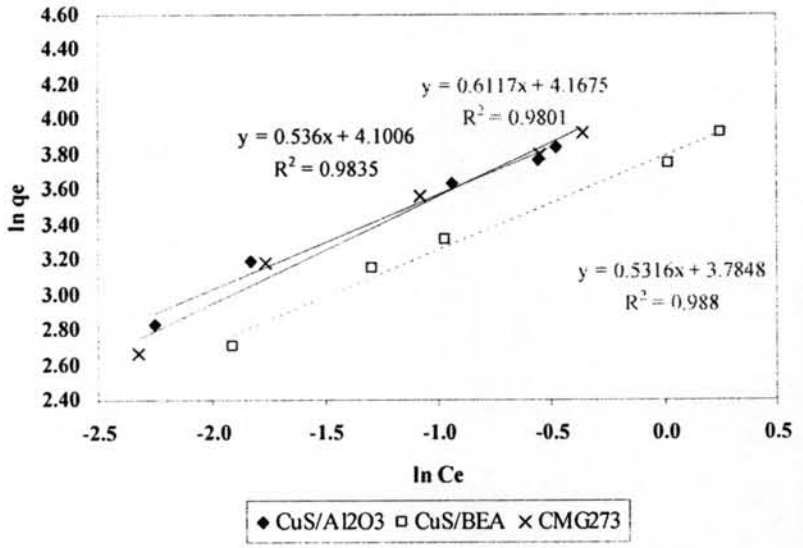


**Figure 4.13** Freundlich adsorption isotherm for metallic mercury removal at 50°C.

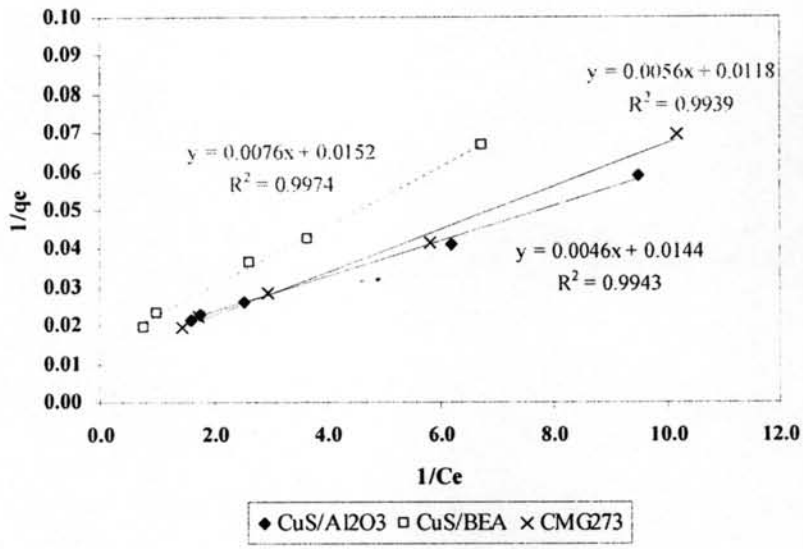


**Figure 4.14** Langmuir adsorption isotherm for metallic mercury removal at 50°C.

It can be concluded from the constants given in Table 4.5 that the equilibrium data fit the Langmuir isotherm model quite well under all conditions studied in the present work. The value of $q_{max}$ obtained from the Langmuir isotherm equation follows the sequence CMG273 (84.75 μmole/g) > $CuS/Al_2O_3$ (69.44 μmole/g) > CuS/BEA (65.79 μmole/g).

Furthermore, the Langmuir parameters can be used to predict the affinity between the adsorbate and adsorbent using the dimensionless separation factor, $R_L$, defined by Hall et al. (1966) as:

$$R_L = \frac{1}{1 + bC_0} \tag{4.16}$$

where $C_0$ is the initial concentration of mercury in μg/L. The criteria shown in Table 4.6. The values of $R_L$ for adsorption of metallic mercury are shown in Figure 4.15.

**Table 4.6** Characteristics of adsorption Langmuir isotherms

| Separation factor, $R_L$ | Characteristics adsorption Langmuir isotherm |
|---|---|
| $R_L > 1$ | Unfavorable |
| $R_L = 1$ | Linear |
| $0 < R_L < 1$ | Favorable |
| $R_L = 0$ | Irreversible |

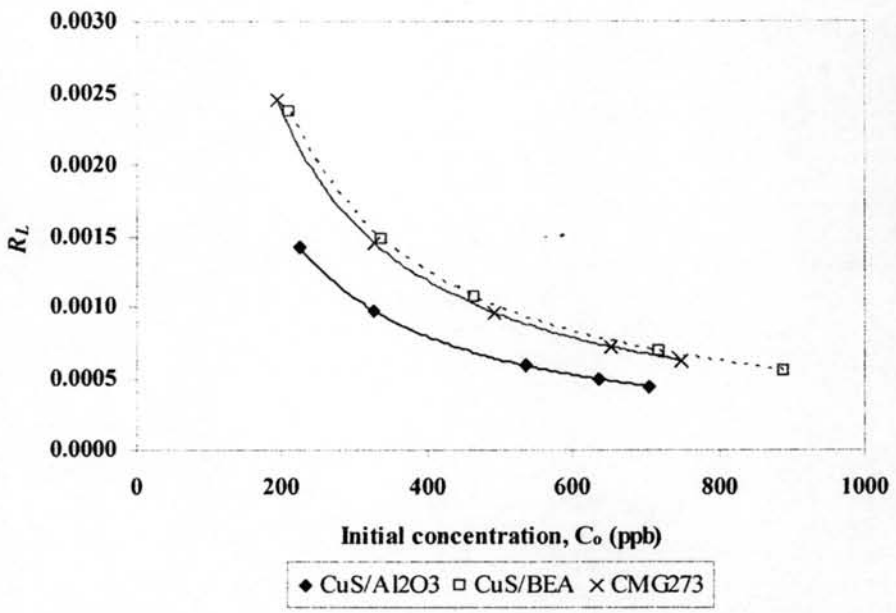


**Figure 4.15** Separation factor of metallic mercury adsorbed at 50°C.

Figure 4.15 indicates that adsorption of metallic mercury is favorable on the all adsorbents and it is more favorable at higher initial concentration of metallic mercury more than for the lower ones.

### 4.7 Pilot Plant Testing

The breakthrough curves of metallic mercury removal in heavy naphtha at concentration of 1000 ppb were conducted in a pilot plant (U844 at the IFP, France) by using CuS/BEA and $CuS/Al_2O_3$. Since the experiments were limited by time, incomplete breakthrough curves were observed for all adsorbents as shown in Figure 4.16.

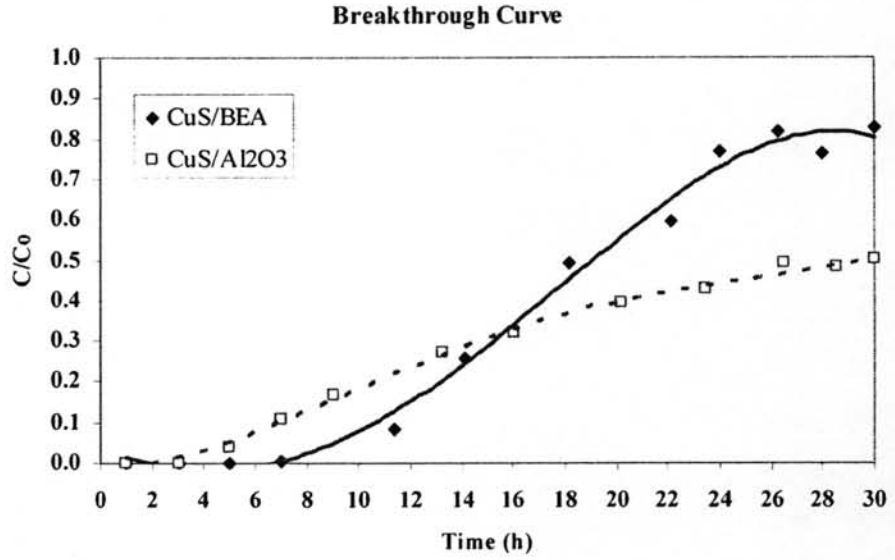


**Figure 4.16** The breakthrough curves for metallic mercury removal at conditions of: concentration of 1000 ppb, 50°C, 7 bar, and 2 ml/min in feed velocity.

From Figure 4.16, the breakthrough time, defined as 5% of the effluent concentration to the initial concentration ($C/C_o$), was 5 and 9 h for $CuS/Al_2O_3$ and CuS/BEA, respectively. In addition, the shape of a breakthrough curve indicated that CuS/BEA exhibited shorter mass transfer zone than $CuS/Al_2O_3$. This result was quite the same as the result from kinetics of adsorption that showed faster pseudo second rate constant and pore diffusion rate for CuS/BEA than $CuS/Al_2O_3$. This may be due to the difference in nature of the surface of the adsorbent which is less polar for CuS/BEA than $CuS/Al_2O_3$, as mentioned in part 4.4.